Analytical Methods

ROYAL SOCIETY OF CHEMISTRY

PAPER

View Article Online
View Journal

Cite this: DOI: 10.1039/d5ay01384d

Enhanced protein binding to off-stoichiometry thiol–ene microfluidic devices: a novel linker approach

Rihards Ruska, *[a] Edmunds Zutis,[a] Kaspars Tars,[b] Andris Kazaks,[b] Gunita Paidere,[a] Janis Cipa,[a] Igor Vozny,[c] Toms Freimanis,[c] Maira Elksne,[a] Anatolijs Sarakovskis,[a] Raivis Zalubovskis [cd] and Andris Anspoks [a]

Microfluidic devices have proven to be a valuable innovation in medical and biological research, offering a fast and efficient platform for testing. Among the materials used for constructing microfluidic channels, off-stoichiometry thiol–ene (OSTE) polymers are especially promising due to their ease of fabrication and lower small-molecule absorption compared to the current gold-standard material, polydimethylsiloxane (PDMS). However, some studies have indicated that there are challenges with binding molecules to the surface thiol groups as they are easily oxidized in air. In this study, a novel linker was synthesized and evaluated for its performance at binding proteins to the surface of OSTE polymer, using a custom-built spectroscopic measurement system. In addition, the results obtained were compared to regular enzyme-linked immunosorbent assay (ELISA) plates and performance of the linker in functionalized microfluidic chips was investigated. Our results indicate that the synthesized linker binds proteins to the OSTE surface and can offer a similar performance to ELISA plates in protein concentration tests highlighting its potential for use in microfluidic chip functionalization.

Received 19th August 2025
Accepted 18th September 2025

DOI: 10.1039/d5ay01384d

rsc.li/methods

1. Introduction

Microfluidic devices have emerged as a promising tool for biomedical applications, especially in diagnostics, as they reduce the need for manual handling enabling higher throughput of analysis and treatments.[1] The use of such devices allows for the manipulation of miniature volumes of liquids in a precise, automated and controlled manner, allowing for execution of multiple experiments in parallel and minimizing the errors introduced by manual labor.[2] Most microfluidic devices are made of polymer materials, with polydimethylsiloxane (PDMS) being the current state-of-the-art material[3] due to its biocompatibility, low cost, optical transparency and ease of fabrication.[4] Despite these advantages, PDMS is known to have limited scalability potential, high absorption of lipophilic molecules and insufficient mechanical robustness for certain configurations.[5,6]

Off-stoichiometry thiol–ene polymer (OSTE) presents a promising alternative to PDMS within the field of microfluidics. OSTE polymers are based on UV-curable thiol–ene chemistry utilizing off-stoichiometry ratios, which allow for a single-step structuring *via* standard photolithographic techniques.[7] OSTE offers ease of fabrication and scalability, tunable mechanical properties, ease of bonding without additional treatment and reduced small molecule absorption as compared to PDMS.[8] Compared to other UV-curable polymers, OSTE also shows resistance to oxygen inhibition and low shrinkage of structures.[9] Furthermore, OSTE fabrication processes can be easily upscaled *via* reaction injection molding, allowing for scalable manufacturing of such devices.[10] Recently various literature sources reported OSTE material being used for various applications – from organ-on-chip[11] and microneedle arrays[12] to biosensors.[13]

However, despite the advanced properties of OSTE, devices made solely from this material are associated with a challenge to establish secure connections to tubing, which can induce leakage, along with significant light scattering. Nevertheless, hybrid devices made from cyclic olefin copolymer (COC)/OSTE have been shown as a promising alternative to facilitate increased optical transparency and a reliable leak-free connection mechanism between the microfluidic chip and tubing while still providing biocompatibility and low particle absorbance. While custom COC patterning itself requires costly and complicated processing techniques, COC–OSTE hybrid device fabrication allows simple fabrication due to the ease of bonding between the polymer surfaces.[14,15]

[a]Institute of Solid State Physics, University of Latvia, 8 Kengaraga Street, LV-1063, Riga, Latvia. E-mail: rihards.ruska@cfi.lu.lv
[b]Latvian Biomedical Research and Study Centre, 3 Ratsupites Street, LV-1048, Riga, Latvia
[c]Latvian Institute of Organic Synthesis, 21 Aizkraukles Street, LV-1006, Riga, Latvia
[d]Institute of Chemistry and Chemical Technology, Faculty of Natural Sciences and Technology, Riga Technical University, 3 P. Valdena Street, LV-1048 Riga, Latvia

OSTE surfaces have been functionalized using a variety of strategies, primarily involving click-chemistry to link molecules to the excess thiol groups on the OSTE surface after polymerization. This method allows for the attachment of detection molecules, such as enzymes,[16] aptamers,[17] antibodies,[13] and nanoparticles,[18] to capture the target molecule.[19] Nevertheless, surface thiol groups are prone to oxidation in air, making devices based on these reactions unsuitable for storage and operation for prolonged periods in a regular atmosphere.[20] Similarly, click chemistry has been employed for OSTE functionalization *via* allyl groups to immobilize proteins such as pepsin[21] and galactose oxidase.[22] A commonly reported protocol here involves multiple consecutive steps, including the preparation of protected 2-aminoethanethiol, its attachment to the surface, deprotection, coupling with ascorbic acid, and final protein immobilization.

To make OSTE devices more robust, easy-to-use linkers with stable reactive groups for protein binding must be developed and employed. A potential approach to achieve protein binding is synthesis and use of $-NH_2$ reactive linkers, which can directly bind to the more stable double bonds on the OSTE surface.[20] In our study, we have designed and synthesized a novel linker capable of both – binding to the OSTE surface *via* reaction with double bond and subsequently selectively interacting with $-NH_2$ group of proteins thus anchoring the protein on the surface. We applied it for the detection of human carbonic anhydrase IX (CA IX) on the OSTE surface.

CA IX is a well-known biomarker for hypoxic forms of cancer.[23] It is overproduced in many tumors including renal cell carcinoma,[24] malignant melanoma, lung carcinoma, breast cancer[25] and others. CA IX is a membrane protein, rarely found on the surface of normal cells, and limited to the tissue of gastrointestinal tract.[26] Furthermore, elevated expression of CA IX is generally associated with poor prognosis and reduced disease-free interval following successful therapy. However, the diagnostic potential of CA IX has been underutilized. It is known that although CA IX is a membrane protein, it can also be found in free form in body fluids, presumably due to proteolytic cleavage of its extracellular domains.[27]

Free CA IX has been previously detected in blood and urine.[27,28] It has been demonstrated that the free CA IX levels in cancer patients are higher compared to healthy individuals.[28] Therefore, detecting free CA IX could be useful for monitoring the presence of tumor cells, *e.g.*, after surgery or chemotherapy using minimally invasive or non-invasive techniques. The overall amount of circulating free CA IX is low, therefore development of highly sensitive detection techniques for CA IX is a crucial task. Typically, free CA IX levels are detected by immunoprecipitation, enzyme-linked immunosorbent assay (ELISA) or western blot, all of which are time-consuming methods, not easily performed in ambulatory settings.

Herein, we demonstrate a novel strategy for optical detection of human CA IX levels in samples using linker functionalized OSTE/COC devices and using horseradish peroxidase (HRP) catalyzed reaction of an enhanced chemiluminescence (ECL) substrate. The results of this detection method were compared with those of functionalized OSTE cylinders and standard ELISA. The presented device holds potential to be used for rapid detection of human CA IX and other antigens significantly reducing detection time compared to standard detection procedures.

2. Materials and methods

2.1. Synthesis of the linker

Unless otherwise stated, all reagents, starting materials and solvents were obtained from commercial sources and used as received. Analytical thin-layer chromatography was performed on silica gel, spots were visualized with UV light (254 and 365 nm). Nuclear magnetic resonance (NMR) spectra were recorded in parts per million from internal tetramethylsilane (TMS) on the δ scale. ^{1}H and ^{13}C NMR spectra were recorded in $CDCl_3$ on a Bruker Avance Neo 400 MHz spectrometer. All chemical shift values are quoted in ppm and coupling constants quoted in Hz. High-resolution mass spectra (HRMS) were recorded on a mass spectrometer with a Q-TOF micro mass analyzer using the ESI technique. The overall synthesis scheme is illustrated in Fig. 1.

2.1.1. Nonan-9-ol pivalate (3). 1,9-Nonanediol (**2**) (10.0 g, 62.4 mmol, 1 equiv.) was dissolved in dry THF (80 mL), then DMAP (198 mg, 1.62 mmol, 0.025 equiv.) and pyridine (880 mg, 11.2 mmol, 0.18 equiv.) were added to the mixture. The mixture was cooled in an ice bath and pivaloyl chloride (9.03 g, 74.9 mmol, 1.2 equiv.) was added portion wise and the mixture was stirred at room temperature (RT) for 18 h. The mixture was diluted with dry diethyl ether (200 mL) and water (150 mL). The organic layer was separated, and the aqueous layer was extracted with diethyl ether (2 × 100 mL). The combined organic layers were washed with sat. sodium bicarbonate solution (100 mL) and water (100 mL). Volatiles were evaporated in vacuum and the residue was purified on silica gel column PE/EtOAc (5 : 1). Compound **3** (6.48 g, 43%) was obtained as a colorless oil.

^{1}H NMR (400 MHz, $CDCl_3$) δ 4.04 (t, J = 6.7 Hz, 2H), 3.63 (t, J = 6.6 Hz, 2H), 1.64–1.52 (m, 4H), 1.38–1.28 (m, 10H), 1.19 (s, 9H).

^{13}C NMR (101 MHz, $CDCl_3$) δ 178.8, 64.6, 63.2, 38.9, 32.9, 29.6, 29.4, 29.3, 28.7, 27.3, 26.0, 25.8.

2.1.2. 9-Nonanoic acid pivalate (4). Nonan-9-ol pivalate (**3**) (2.00 g, 8.18 mmol, 1 equiv.) was dissolved in dry acetone (50 mL). CrO_3 (1.64 g, 16.4 mmol, 2 equiv.) was dissolved in 5 M H_2SO_4 (4.5 mL) and cooled in an ice bath. The acetone solution was added very slowly dropwise to the chrome(VI) oxide solution. The reaction was left with stirring in the melting ice bath overnight. To the mixture water (200 mL) was added and it was extracted with diethyl ether (3 × 100 mL). The combined organic layers were washed with 1 M HCl (50 mL) and water (50 mL) and dried over Na_2SO_4. Volatiles were evaporated in vacuum. Compound **4** (1.50 g, 71%) was obtained as a slight yellow oil.

^{1}H NMR (400 MHz, $CDCl_3$) δ 4.04 (t, J = 6.7 Hz, 2H), 2.34 (t, J = 7.5 Hz, 2H), 1.66–1.56 (m, 4H), 1.38–1.28 (m, 8H), 1.19 (s, 9H).

^{13}C NMR (101 MHz, $CDCl_3$) δ 179.7, 178.9, 64.6, 38.9, 34.1, 29.2, 29.1, 29.0, 28.7, 27.3, 26.0, 24.8.

2.1.3. 9-Hydroxy nonanoic acid (5). 9-Nonanoic acid pivalate (**4**) (1.50 g, 5.80 mmol, 1 equiv.) was dissolved in THF (12

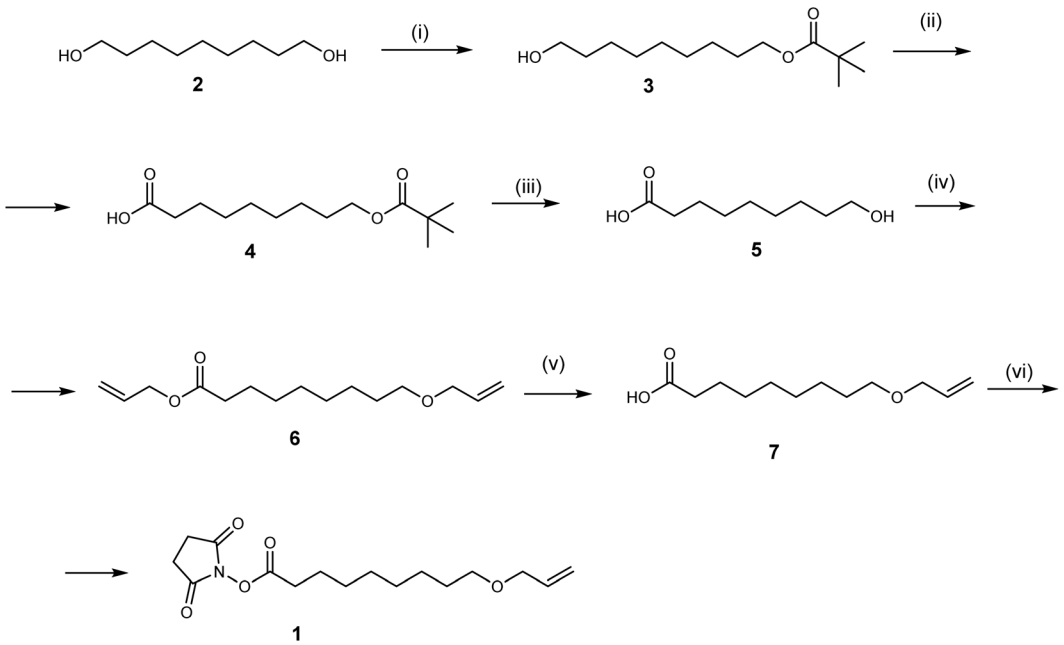

Fig. 1 Schematic illustration of synthesis conditions and reagents: (i) 2,2-dimethylpropanoyl chloride, DMAP, pyridine, THF, rt, 16 h, 43%; (ii) CrO_3, H_2SO_4, acetone, 0 °C, 16 h, 71%; (iii) LiOH, THF, H_2O, 40 °C, 16 h, 99%; (iv) allyl bromide, NaOH, DMF, rt, 16 h, 44%; (v) KOH, MeOH, rt, 1 h, 88%; (vi) *N*-hydroxysuccinimide, EDC·HCl, DMAP, CH_2Cl_2, 0 °C to rt, 16 h, 81%.

mL) and H_2O (28 mL), then LiOH·H_2O (2.44 g, 59.1 mmol, 10 equiv.) was added to the solution. The reaction was stirred at 60 °C for 18 h. The reaction mixture was quenched with 1 M HCl solution, acidified to pH 2 and extracted with diethyl ether (3 × 40 mL). The combined organic layers were washed with water (3 × 30 mL) and dried over Na_2SO_4 and evaporated in vacuum followed by evacuation of residual volatiles at 60 °C (2 mbar). Compound **5** (1.00 g, 99%) was obtained as a slight yellow oil.

^{1}H NMR (400 MHz, $CDCl_3$) δ 6.88 (br s, 1H), 3.64 (t, J = 6.5 Hz, 2H), 2.34 (t, J = 7.4 Hz, 2H), 2.17 (s, 1H), 1.69–1.49 (m, 4H), 1.40–1.27 (m, 8H).[29]

2.1.4. Allyl 9-(allyloxy)nonanoate (6). 9-Hydroxy nonanoic acid (**5**) (1.00 g, 5.80 mmol, 1 equiv.) was dissolved in dry DMF (15 mL) and cooled in an ice bath. Then 60% NaH in mineral oil (696 mg, 17.4 mmol, 3 equiv.) was added to the mixture and stirred for 1 h in the ice bath. Allyl bromide (2.51 mL, 29.0 mmol, 5 equiv.) was added dropwise to the solution and it was stirred at RT for 18 h. The mixture was diluted with water (50 mL) and extracted with diethyl ether (3 × 50 mL). The combined organic extract was washed with brine (2 × 30 mL) and water (30 mL) and dried over Na_2SO_4. The volatiles were evaporated in vacuum and the residue was purified on silica gel column PE/EtOAc (2 : 1). Compound **6** (650 mg; 44%) was obtained as a colorless oil.

^{1}H NMR (400 MHz, $CDCl_3$) δ 5.91 (ddtd, J = 17.0, 10.4, 5.7, 1.0 Hz, 2H), 5.36–5.12 (m, 4H), 4.57 (dt, J = 5.7, 1.4 Hz, 2H), 3.95 (dt, J = 5.6, 1.4 Hz, 2H), 3.41 (t, J = 6.7 Hz, 2H), 2.32 (t, J = 7.5 Hz, 2H), 1.68–1.51 (m, 3H), 1.39–1.28 (m, 3H), 1.31 (s, 6H).

^{13}C NMR (101 MHz, $CDCl_3$) δ 173.6, 135.2, 132.5, 118.2, 116.8, 71.9, 70.6, 65.1, 34.4, 29.9, 29.4, 29.3, 29.2, 26.3, 25.1.

2.1.5. 9-(Allyloxy)nonanoic acid (7). To the solution of allyl 9-(allyloxy)nonanoate (**6**) (315 mg, 1.24 mmol, 1 equiv.) in MeOH/H_2O (3 : 1) (10 mL) add KOH (208 mg, 3.72 mmol, 3 equiv.). The mixture was stirred at RT for 1 h. The mixture was acidified with conc. HCl to pH 4, and the volatiles were evaporated in vacuum. The residue purified on silica gel column CH_2Cl_2/MeOH (9 : 1). Compound **7** (233 mg, 88%) was isolated as colorless oil.

^{1}H NMR (400 MHz, $CDCl_3$) δ 9.1 (br s, 1H), 5.91 (ddt, J = 17.2, 10.4, 5.6 Hz, 1H), 5.26 (dq, J = 17.2, 1.7 Hz, 1H), 5.16 (dq, J = 10.4, 1.3 Hz, 1H), 3.96 (dt, J = 5.6, 1.4 Hz, 2H), 3.42 (t, J = 6.7 Hz, 2H), 2.34 (t, J = 7.5 Hz, 2H), 1.68–1.52 (m, 3H), 1.40–1.17 (m, 9H).

2.1.6. 2,5-Dioxopyrrolidin-1-yl 9-(allyloxy)nonanoate (1). To ice-cold solution of 9-(allyloxy)nonanoic acid (**7**) (233 mg, 1.09 mmol, 1 equiv.) in dry CH_2Cl_2 (30 mL) *N*-hydroxysuccinimide (189 mg, 1.64 mmol, 1.5 equiv.), DMAP (266 mg, 2.18 mmol, 2 equiv.) and EDC·HCl (313 mg, 1.64 mmol, 1.5 equiv.) were added. The mixture was stirred in melting ice-bath for 16 h. Extra CH_2Cl_2 (70 mL) was added, and the mixture was washed with 1 M HCl (10 mL) and sat. $NaHCO_3$ (20 mL). Solvent was evaporated in vacuum. The residue was purified on silica gel column CH_2Cl_2/MeOH (19 : 1). Compound **1** (276 mg, 81%) was isolated as colorless oil, which slowly solidifies.

^{1}H NMR (400 MHz, $CDCl_3$) δ 5.91 (ddt, J = 17.2, 10.4, 5.6 Hz, 1H), 5.26 (dq, J = 17.2, 1.7 Hz, 1H), 5.15 (dq, J = 10.4, 1.4 Hz, 1H), 3.95 (dt, J = 5.6, 1.4 Hz, 2H), 3.41 (t, J = 6.7 Hz, 2H), 2.82 (s, 4H), 2.59 (t, J = 7.5 Hz, 2H), 1.79–1.67 (m, 2H), 1.63–1.51 (m, 2H), 1.46–1.27 (m, 8H).

^{13}C NMR (101 MHz, $CDCl_3$) δ 169.3, 168.8, 135.2, 116.8, 71.9, 70.5, 31.1, 29.8, 29.3, 29.1, 28.8, 26.2, 25.7, 24.7.

HRMS (ESI) $[M + Na]^+$: m/z for ($C_{16}H_{25}NO_5Na$) 334.1630. Found 334.1622.

2.2. Soft lithography mold preparation

A stereolithography 3D printer (Formlabs, Form 3+) was utilized to fabricate a double inverted mold (Grey resin V4, Formlabs). Inverted mold was fabricated using Silicone Elastomer polydimethylsiloxane (PDMS, Sylgard TM 184), which was mixed at a 1 : 10 (w/w), using a planetary mixer at 500 rpm for 1 minute. The mixture was then poured into the 3D-printed mold and vacuum degassed. For curing, the mold was covered with a polyethylene terephthalate (PET) film, placed in a custom holder and heated at 60 °C for 3 h. Once cured, the mold was carefully demolded, cleaned with 2-propanol, and dried with nitrogen.

2.3. Fabrication of linker functionalized OSTE cylinders

Commercial OSTE components (Mercene Labs, Ostemer 220, Reagent A and Reagent B) were mixed at a 1.86 : 1 ratio in a planetary mixer at 750 rpm for 5 minutes (axial rotation fraction 1/2.5), followed by a 5-minute degassing step at 750 rpm (axial rotation fraction 1/36.7). Subsequently, the prepared mixture was poured into a conical centrifuge tube and degassed in a vacuum chamber for 0.5 to 1 hour.

A glass slide was used as a substrate for the sample by capping the PDMS mold, which was then clamped in a custom jig. OSTE was used to fill the mold cavity with a pressure system (OB1 MK3+, Elveflow) using 1000 mbar pressure. After filling, OSTE was cured under 300 mJ cm^{-2} UV light using a Mask Aligner (Suss, model MA6) with ND33 and I-line filters to set dose rate to 6 mJ s^{-1}. The assembly, consisting of the glass slide with the interconnected OSTE cylinders, was then extracted from the mold. The cylinders were separated by trimming away the interconnecting excess OSTE polymer[20] (Fig. 2a).

To functionalize the surface of the OSTE cylinders with a linker, a 10 mM linker solution was prepared in acetone (Purris p.a). Acetone was chosen as a solvent as it efficiently dissolved the linker, promoted surface wetting and evaporated after the functionalization. Water and 2-propanol could not sufficiently dissolve the linker while less polar, chlorinated solvents were not used due to environmental and health concerns. 100 μL of the linker solution was then deposited onto each OSTE cylinder. For the control (unfunctionalized) samples, 100 μL of pure acetone was used. The samples were then exposed to 4000 mJ cm^{-2} UV light using ND33 and i-line filters to promote immobilization of the linker to the OSTE surface. After exposure, samples were rinsed under a deionized water (DIW) stream and blow-dried under nitrogen flow.

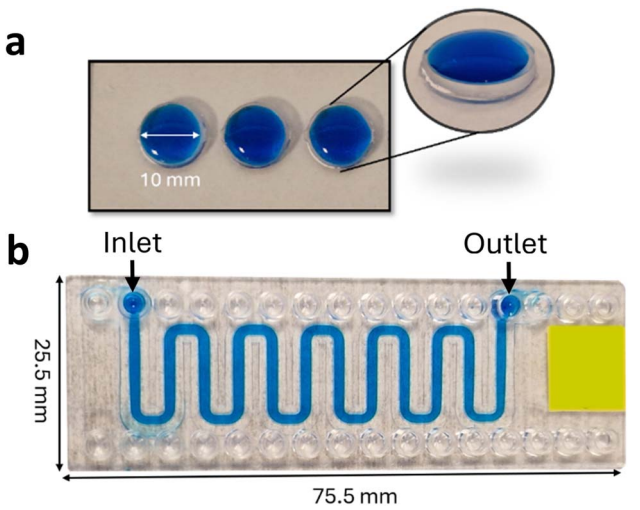

Fig. 2 Design and dimensions of: (a) OSTE cylinders and (b) microfluidic chips.

2.4. Fabrication of linker functionalized OSTE microfluidic chips

OSTE/COC microfluidic chips were fabricated using commercial OSTE as sidewalls and COC as the substrate similar to previously reported protocols.[10,14,15] In short, 2 component silicone elastomer QSil 216 (CHT, Germany) was cast into a double-inverse 3D-printed mold as previously described. The resulting negative QSil mold was capped with a COC slide with mini Luer ports (microfluidic ChipShop) and then clamped in a custom jig. The mold cavity was filled with OSTE polymer under 800 mbar pressure (OB1 MK3+, Elveflow) and cured with a 75 mJ cm^{-2} dose of UV radiation (Suss, model MA6). Following curing, a 140 μm COC film was treated with oxygen plasma (800 sccm O_2, 700 W, 0.133 mbar for 5 min), while the device with OSTE sidewalls were heated to 60 °C. The plasma-treated COC film was then bonded to the OSTE layer, clamped, and cured with a UV dose of 425 mJ cm^{-2} (Suss, model MA6). The result was a chip with bent, 370 mm long, 1.5 × 0.5 mm rectangular microfluidics channel (Fig. 2b).

Subsequently, the clamped device was filled with a 10 mM linker solution in acetone, channels were sealed, and the entire device was exposed to 4000 mJ cm^{-2} of UV radiation using an i-line and ND33 filters (Suss, model MA6). After curing, the device was rinsed with 5 mL of acetone, 5 mL of DIW and blow-dried with air. This process resulted in OSTE/COC devices with linker molecules bound to the channel sidewalls.

2.5. Protein immobilization to the sample surface

For protein binding and OSTE aging tests, horseradish peroxidase (HRP) solution in phosphate-buffered saline (PBS, 1 mg mL^{-1}, P8250-25KU, Sigma-Aldrich) was prepared and used. Cylindrical OSTE samples were incubated with 100 μL of the HRP solution deposited onto their surface for 2 hours at RT. After consecutive thorough rinsing under DIW stream, 75 μL of substrate mix from the ECL substrate kit (Ultra High Sensitivity (ab133409), Abcam) was applied to the cylinder, and spectroscopic measurements were performed as described below.

For human CA IX limit of detection (LOD) tests on OSTE cylinders, CA IX antibody pair (capture antibodies (CAb) and unconjugated detection antibodies (DAb) (ab253844), Abcam) was used. CAb were chemically coupled to OSTE cylinders, followed by the capture of CA IX and detection by HRP labeled DAb. CA IX was produced and purified as described previously.[30] To enable downstream detection, DAb were conjugated to HRP using HRP kit (ab102890, Abcam) according to manufacturer's instructions.

To bind CAb to OSTE, 75 μL of CAb (1 μg mL^{-1}) solution in (PBS) was applied to functionalized OSTE cylinder and incubated for 30 minutes at RT. Rinsing after this and successive incubation steps was performed under DIW steam. To block unreacted linker, cylinders were further incubated with 100 μL of 1% bovine serum albumin (BSA) in PBS-Tween (0.1% Tween-20 in PBS) for 60 minutes at RT. Cylinders were rinsed and further incubated with 75 μL of CA IX at desired concentrations in the PBS buffer for 30 minutes at RT. After rinsing, 50 μL of HRP labelled DAb solution (DAb-HRP, 1 μg mL^{-1}) in PBS was applied to cylinders and incubated for 30 minutes at RT. After thorough rinsing, 20 μL of substrate mixture from ECL substrate kit was applied to cylinders center and spectroscopic measurements were performed as described in section 2.6.

The same order of protein solution application and their incubation time was used to bind proteins to the walls inside of the microfluidic chip channels. The volume of applied reagents was 100 μL as the solutions were applied using 1 mL syringe with adapters (10001765, ChipShop). Rinsing in between the steps was done with 1 mL of PBS, followed by blowing out excess fluid with 3 mL of air using a syringe.

The ELISA test was performed using the same overall protocol as for the assays conducted on OSTE cylinders, with the main difference being that CAb were immobilized on commercial ELISA plates (Greiner, Meiningen, Germany) by overnight incubation in carbonate buffer. Detection was carried out using a colorimetric readout based on *O*-phenylenediamine dihydrochloride (P6912-100TAB, Sigma, Burlington, MA, USA).

2.6. Spectroscopic measurements

Since OSTE cylinders and microfluidic chips were custom-made, a custom measurement system was constructed to reliably measure the luminescent signals from these samples (Fig. 3). It consisted of aluminum breadboard (MB2530/M, Thorlabs), photomultiplier tube (H8259-01, Hamamatsu), complimentary photon counting unit (C8855-01, Hamamatsu), neutral density optical filters (NE10B, NE20B, NE30B and NE40B, Thorlabs), optical filter holders (CFS1/M and CFS1-F1, Thorlabs), blacked out box (based on EKET, IKEA), 3D printed sample holder as well as various optical element connectors. The optical signal was registered using LabVIEW program provided with photon counting unit C8855-01. The measured spectral data was then processed and illustrated using program Origin Pro 2024.

For ELISA plates, optical density was measured spectrophotometrically at 492 nm using an ELISA plate reader (BDSL Immunoskan MS, Finland). A positive signal was defined relative to the negative control, *i.e.*, the mean OD429 values from the wells probed with all reagents except CA IX.

3. Results

3.1. Linker performance tests

To gain understanding of the synthesized linker performance, OSTE samples were prepared with and without functionalization with the linker. The samples were incubated with HRP solution and tested for their luminescent properties. The resulting spectra were integrated (Fig. 4a, 1 day) from 30th to 60th second to exclude the rapidly changing range (1st to 30th second) as its integral value was heavily influenced by deviations in time intervals between HRP application and measurement initiation. The results showed that the luminescence intensity of samples functionalized with linker was 4-fold higher than that of regular OSTE samples. Since luminescence intensity is directly proportional to the number of luminescent centers, one can conclude that the linker functionalized samples bound $\sim 10^4$ times more protein molecules than the unfunctionalized samples. The proposed mechanism of the linker performance is shown in Fig. 4b.

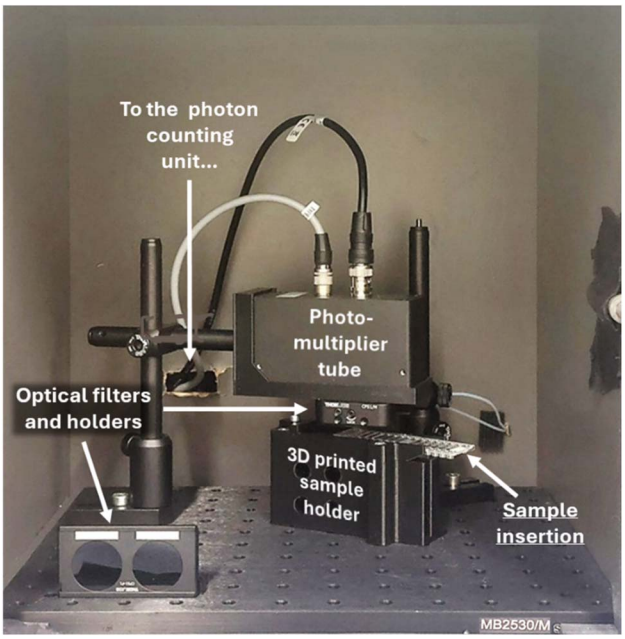

Fig. 3 Image of the custom measurement system.

For some applications it could be crucial to understand the stability of the linker functionalized samples. To quantify that, samples were prepared and aged for 1 day, 1 month and 9 months. During the aging, samples were kept in a dark place, in Petri dishes, at RT. All samples were then measured on the same day for their HRP binding properties. As shown in Fig. 4a, increased storage time resulted in better protein binding. We speculate that the increase was a result of acetone and other molecule desorption from the OSTE surface over time, which uncovered more linker molecules for protein binding. Nevertheless, these results show that linker functionalized samples can maintain their binding performance for at least 9 months.

3.2. Comparison of CA IX LOD for OSTE cylinders and ELISA plates

One potential application for protein-binding OSTE surfaces in microfluidic chips is measuring protein concentrations. Since most current protein concentration tests utilize ELISA plates, comparing the LOD of CA IX on protein-binding OSTE to the

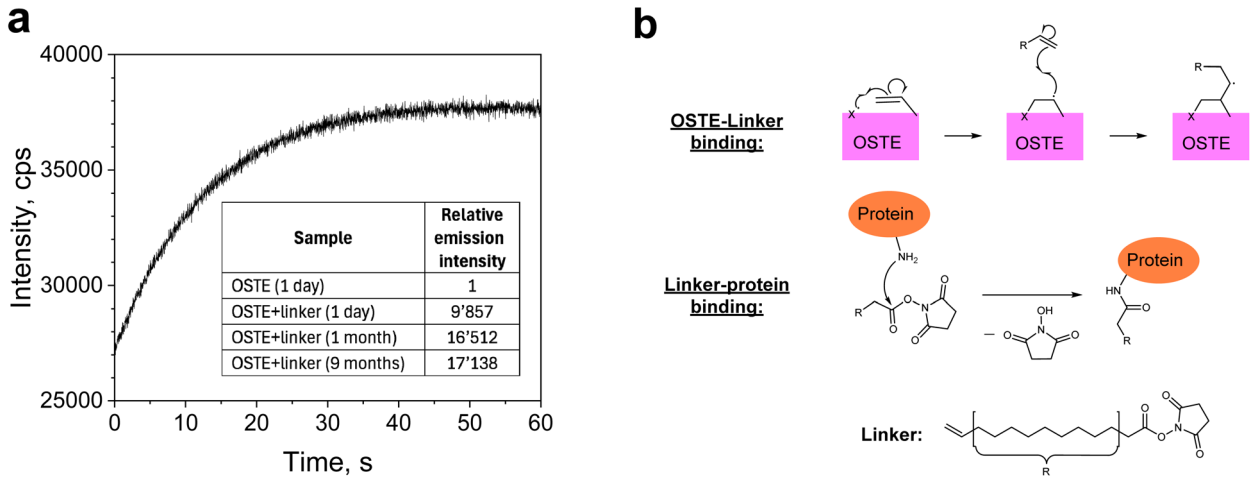

Fig. 4 (a) HRP catalyzed chemiluminescence intensity graph (OSTE + linker, 1 day) and relative emission intensities of samples aged for 1 day, 1 month and 9 months respectively. (b) Proposed mechanism of linker attachment to the OSTE surface and protein immobilization mechanism to the linker, where X is a photo-generated radical species (possibly a leftover photoinitiator molecule from the initial OSTE polymerization[20] or radicals generated through C–S bond cleavage[31,32]).

results of ELISA plates could help evaluate the feasibility of linker approach.

To assess the linker's performance against standard ELISA tests, a batch of cylindrical, functionalized OSTE samples was produced and spectroscopic measurements for various CA IX protein concentrations were performed (Fig. 5a). The results showed that functionalized OSTE tests yielded a similar LOD to the ELISA plate tests – 10 ng mL^{-1} and 9 ng mL^{-1}, respectively (Fig. 5b). However, the background signal for OSTE samples was noisier than that of ELISA plates. This could be explained by variations in OSTE sample production as well as their treatment with solutions and subsequent rinsing. For potentially lower noise signal, future effort must be put toward developing a more controlled rinsing protocol.

Nevertheless, obtained results indicate that for measuring CA IX protein concentrations, linker functionalized OSTE can offer a similar performance to the ELISA plate tests.

3.3. CA IX LOD for microfluidic chips

Since it was determined that the linker functionalized OSTE can indeed bind proteins and offer a similar LOD of CA IX to ELISA plates, to understand the performance and limitations of protein binding in microfluidic chips, CA IX LOD tests were performed on them. The results are illustrated in Fig. 6. CA IX LOD in the microfluidic chips was observed to be similar to OSTE cylinders and ELISA plates – around 10 ng mL^{-1}. Nevertheless, an increase in background signal intensity when compared to the OSTE cylinders was observed. It could be attributed to both the larger surface area of the chip channels and increased concentration of proteins along the edges of the cross-sectionally rectangular channels influenced by decreased mobility of their solutions due to the laminar flow inside the chips. Similarly to the OSTE cylinders, future efforts must be put towards reducing the background noise, for example, by introducing more thorough rinsing steps. Although such

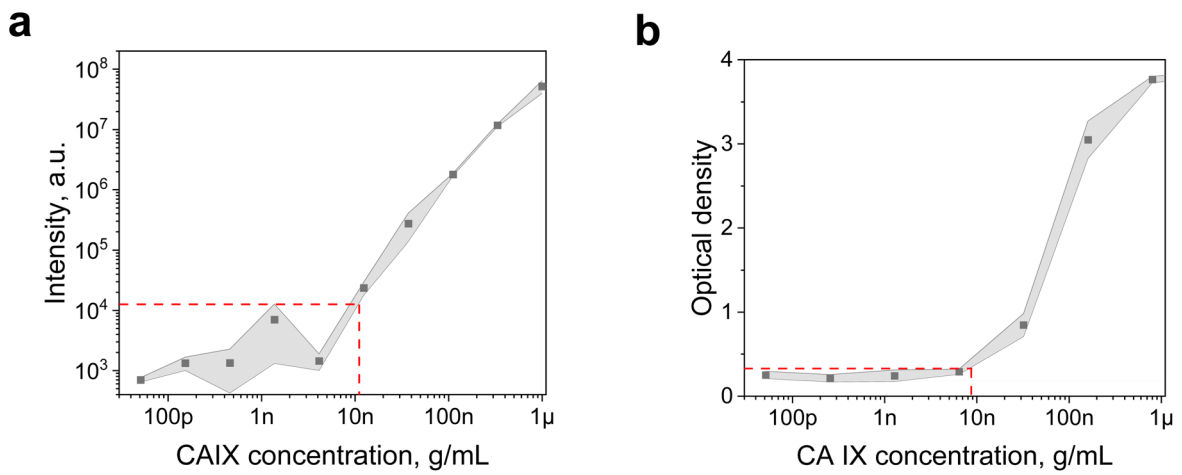

Fig. 5 Average integral luminescent intensity and standard deviation as a function of CA IX concentration for: (a) functionalized, cylindrical OSTE samples, (b) ELISA plate wells.

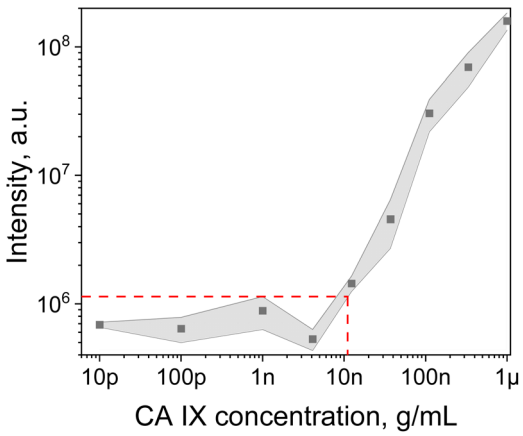

Fig. 6 Average integral luminescent intensity and standard deviation of the linker functionalized OSTE microfluidic chips as a function of CA IX concentrations.

strategy would increase the overall device processing time, it could potentially help to increase the signal-to-noise ratio.

Our results show that by utilizing the novel synthesized linker, one can enhance OSTE protein binding properties. Moreover, functionalized OSTE cylinders and microfluidic chips can offer similar performance to standard ELISA plates in determining the CA IX protein concentrations.

In contrast to more complex attachment strategies – such as the biotin–streptavidin approach,[33,34] which typically involves three bonding steps between the surface and the protein (surface–biotin–streptavidin–protein), or ascorbic acid based approach,[21,22] which requires three bonding sites (surface–aminoethanol–ascorbic acid–protein) along with additional steps for amine group protection/deprotection and photoinitiated attachment – our method relies on a simpler two-step linkage (surface–linker–protein) without the need for extra reagents. This streamlined binding pathway not only simplifies the functionalization process but may also offer improved control and reproducibility.

Besides the effectiveness in CA IX immunoassay, this linker might be used as a potentially versatile tool in other studies involving protein immobilization on the OSTE surface. In addition, since the linker maintains its performance for at least 9 months when stored under ambient laboratory conditions, it could be used for long-term protein-related studies and the development of OSTE-based products or tools with extended shelf-life. Moreover, our proposed mechanism shows that this linker attaches to surfaces *via* a double bond radical reaction. This nonspecific reaction could also be applied to other materials, such as the widely used PDMS,[35] whose surfaces can engage in similar radical reactions, thereby enabling them to absorb various proteins as well.

4. Conclusions

A comprehensive study was conducted to explore the potential for enhancing protein binding on OSTE using novel linker. Our key findings are:

(1) Tests were performed on samples with and without the linker functionalization to analyze their protein binding properties. The results showed that linker functionalized samples bound $\sim 10^4$ times more protein molecules than samples with unfunctionalized OSTE surface. Moreover, the functionalized samples were tested for their stability in time. The results showed that not only did samples remain fully functional after 9 months of storage, but also their binding activity increased.

(2) Samples functionalized with linker were evaluated and compared with ELISA plates in CA IX LOD tests. The results showed that while cylindrical OSTE samples had noisier background, the LOD values were quite similar to the ones of ELISA plates ($LOD_{ELISA\ plates} = \sim 9$ ng mL^{-1}, $LOD_{OSTE} = \sim 10$ ng mL^{-1}). This indicates that linker functionalized OSTE surfaces can be used for controlled protein binding.

(3) Since OSTE is used in microfluidic chips as channel sidewalls, CA IX LOD test with linker functionalized microfluidic chips was also performed. While chips exhibited elevated background signal intensity when compared to cylindrical OSTE samples, the obtained LOD figure was similar – approximately 10 ng mL^{-1}.

Given that the newly synthesized linker binds proteins through a nonspecific reaction with the $-NH_2$ groups of the protein, it exhibits potential for use in immobilization and immunoassay of various other proteins. Similarly, because the linker binds to the OSTE surface through a nonspecific radical reaction, it holds a promise for functionalizing other material surfaces that support attachment through double bond/radical reactions.

Author contributions

Conceptualization: Anatolijs Sarakovskis, Raivis Zalubovskis, Andris Anspoks, Kaspars Tars. Methodology: Anatolijs Sarakovskis, Raivis Zalubovskis, Andris Anspoks, Kaspars Tars. Validation: Andris Anspoks, Anatolijs Sarakovskis, Raivis Zalubovskis, Kaspars Tars. Software: Janis Cipa. Formal analysis: Rihards Ruska. Investigation: Rihards Ruska, Edmunds Zutis, Kaspars Tars, Andris Kazaks, Igor Vozny, Janis Cipa, Toms Freimanis. Resources: Anatolijs Sarakovskis, Raivis Zalubovskis, Edmunds Zutis, Rihards Ruska, Kaspars Tars, Andris Anspoks. Data suration: Rihards Ruska. Writing – original draft: Rihards Ruska, Maira Elksne, Raivis Zalubovskis, Edmunds Zutis, Gunita Paidere. Writing – review & editing: Edmunds Zutis, Maira Elksne, Gunita Paidere, Janis Cipa, Raivis Zalubovskis, Kaspars Tars. Visualization: Edmunds Zutis, Rihards Ruska, Raivis Zalubovskis. Supervision: Anatolijs Sarakovskis, Raivis Zalubovskis, Andris Anspoks, Kaspars Tars. Project administration: Andris Anspoks. Funding acquisition: Andris Anspoks.

Conflicts of interest

There are no conflicts of interest to declare.

Data availability

Data for this article, including raw and calculated spectral data are available at Zenodo database at **https://doi.org/10.5281/zenodo.14699683**.

Acknowledgements

This research is funded by the Latvian Council of Science, project "Development of carbonic anhydrase IX test biosensor for cancer screening" No. LZP-2021/1-0584.

References

1 N. Frey, U. M. Sönmez, J. Minden and P. LeDuc, *Nat. Commun.*, 2022, **13**, 1–11.
2 O. Scheler, W. Postek and P. Garstecki, *Curr. Opin. Biotechnol.*, 2019, **55**, 60–67.
3 J. Zhou, D. A. Khodakov, A. V. Ellis and N. H. Voelcker, *Electrophoresis*, 2012, **33**, 89–104.
4 K. M. Raj and S. Chakraborty, *J. Appl. Polym. Sci.*, 2020, **137**, 48958.
5 E. K. Sackmann, A. L. Fulton and D. J. Beebe, *Nature*, 2014, **507**, 181–189.
6 C. F. Carlborg, T. Haraldsson, K. Öberg, M. Malkoch and W. Van Der Wijngaart, *Lab Chip*, 2011, **11**, 3136–3147.
7 E. Borda, D. I. Medagoda, M. J. I. Airaghi Leccardi, E. G. Zollinger and D. Ghezzi, *Biomaterials*, 2023, **293**, 1–13.
8 B. J. van Meer, H. de Vries, K. S. A. Firth, J. van Weerd, L. G. J. Tertoolen, H. B. J. Karperien, P. Jonkheijm, C. Denning, A. P. IJzerman and C. L. Mummery, *Biochem. Biophys. Res. Commun.*, 2017, **482**, 323–328.
9 N. B. Cramer, T. Davies, A. K. O'Brien and C. N. Bowman, *Macromolecules*, 2003, **36**, 4631–4636.
10 N. Sandström, R. Z. Shafagh, A. Vastesson, C. F. Carlborg, W. Van Der Wijngaart and T. Haraldsson, *J. Micromech. Microeng.*, 2015, **25**, 075002.
11 R. Rimsa, A. Galvanovskis, J. Plume, F. Rumnieks, K. Grindulis, G. Paidere, S. Erentraute, G. Mozolevskis and A. Abols, *Micromachines*, 2021, **12**, 1–17.
12 Y. Liu, H. Li, Z. Feng, Z. Chen, M. Zhang, J. Zhou, Q. He, H. Zhang, T. Jiang and W. Guo, in *2024 IEEE 19th International Conference on Nano/Micro Engineered and Molecular Systems, NEMS 2024*, Institute of Electrical and Electronics Engineers Inc., 2024.
13 W. Guo, L. Vilaplana, J. Hansson, M. P. Marco and W. van der Wijngaart, *Biosens. Bioelectron.*, 2020, **163**, 112279.
14 C. Bajo-Santos, M. Priedols, P. Kaukis, G. Paidere, R. Gerulis-Bergmanis, G. Mozolevskis, A. Abols and R. Rimsa, *Int. J. Mol. Sci.*, 2023, **24**, 1–18.
15 M. Priedols, G. Paidere, C. B. Santos, A. Miscenko, R. G. Bergmanis, A. Spule, B. Bekere, G. Mozolevskis, A. Abols and R. Rimsa, *Polymers*, 2023, **15**, 789.
16 E. Çakmakçi, B. Yuce-Dursun and S. Demir, *React. Funct. Polym.*, 2017, **111**, 38–43.
17 S. Bourg, F. d'Orlyé, S. Griveau, F. Bedioui, J. A. F. da Silva and A. Varenne, *Chemosensors*, 2020, **8**, 24.
18 S. Tähkä, J. Sarfraz, L. Urvas, R. Provenzani, S. K. Wiedmer, J. Peltonen, V. Jokinen and T. Sikanen, *Anal. Bioanal. Chem.*, 2019, **411**, 2339–2349.
19 A. B. Lowe, *Polym. Chem.*, 2014, **5**, 4820–4870.
20 R. Ruska, A. Sarakovskis, E. Zutis, G. Paidere, I. Vozny, J. Cipa, J. Gabrusenoks, T. Freimanis, R. Zalubovskis and A. Anspoks, *Materials*, 2024, **17**, 6135.
21 N. Lu, D. Sticker, A. Kretschmann, N. J. Petersen and J. P. Kutter, *Anal. Bioanal. Chem.*, 2020, **412**, 3559–3571.
22 J. P. Lafleur, S. Senkbeil, J. Novotny, G. Nys, N. Bøgelund, K. D. Rand, F. Foret and J. P. Kutter, *Lab Chip*, 2015, **15**, 2162–2172.
23 J. Pastorek and S. Pastorekova, *Semin. Cancer Biol.*, 2015, **31**, 52–64.
24 T. A. Bismar, F. J. Bianco, H. Zhang, X. Li, F. H. Sarkar, W. A. Sakr, D. J. Grignon and M. Che, *Pathology*, 2003, **35**, 513–517.
25 S. K. Chia, C. C. Wykoff, P. H. Watson, C. Han, R. D. Leek, J. Pastorek, K. C. Gatter, P. Ratcliffe and A. L. Harris, *J. Clin. Oncol.*, 2001, **19**, 3660–3668.
26 S. Pastorekova, S. Parkkila, A. K. Parkkila, R. Opavsky, V. Zelnik, J. Saarnio and J. Pastorek, *Gastroenterology*, 1997, **112**, 398–408.
27 J. Závada, Z. Závadová, M. Zat'ovičová, L. Hyršl and I. Kawaciuk, *Br. J. Cancer*, 2003, **89**, 1067–1071.
28 U. Brown-Glaberman, M. Marron, P. Chalasani, R. Livingston, M. Iannone, J. Specht and A. T. Stopeck, *Dis. Markers*, 2016, **2016**, 9810383.
29 C. Chapuis, F. Robvieux, C. Cantatore, C. Saint-Léger and L. Maggi, *Helv. Chim. Acta*, 2012, **95**, 428–447.
30 J. Leitans, A. Kazaks, A. Balode, J. Ivanova, R. Zalubovskis, C. T. Supuran and K. Tars, *J. Med. Chem.*, 2015, **58**, 9004–9009.
31 D. F. McMillen and D. M. Golden, *Annu. Rev. Phys. Chem.*, 1982, **33**, 493–532.
32 X. Q. Yao, X. J. Hou, H. Jiao, H. W. Xiang and Y. W. Li, *J. Phys. Chem. A*, 2003, **107**, 9991–9996.
33 R. Zandi Shafagh, A. Vastesson, W. Guo, W. Van Der Wijngaart and T. Haraldsson, *ACS Nano*, 2018, **12**, 9940–9946.
34 R. Zandi Shafagh, J. X. Shen, S. Youhanna, W. Guo, V. M. Lauschke, W. Van Der Wijngaart and T. Haraldsson, *ACS Appl. Bio Mater.*, 2020, **3**, 8757–8767.
35 Q. Tu, J. C. Wang, Y. Zhang, R. Liu, W. Liu, L. Ren, S. Shen, J. Xu, L. Zhao and J. Wang, *Rev. Anal. Chem.*, 2012, **31**, 177–192.